Current Therapeutic Research 97 (2022) 100682

Contents lists available at ScienceDirect

Current Therapeutic Research

journal homepage: www.elsevier.com/locate/curtheres

Original Research

Use of Magnetic Resonance Imaging to Assess the Regenerative Effects of Adipose Tissue-Derived Mesenchymal Stem Cells in a Rabbit Cartilaginous Laryngeal Defect Model

Kamyar Iravani, MD[1,*], Davood Mehrabani, PhD[2], Aida Doostkam, MD, PhD[3], Negar Azarpira, MD[4], Pooya Iranpour, MD[5], Mohsen Bahador, MD[1], Soheila Mehravar, MD[1]

[1] Otolaryngology Research Center, Department of Otolaryngology, Shiraz University of Medical Sciences, Shiraz, Iran
[2] Stem Cell Technology Research Center, Shiraz University of Medical Sciences, Shiraz, Iran
[3] Shiraz Nephro-Urology Research Center, Shiraz University of Medical Sciences, Shiraz, Iran
[4] Transplant Research Center, Shiraz Institute of Stem Cell and Regenerative Medicine, Shiraz University of Medical Sciences, Shiraz, Iran
[5] Medical Imaging Research Center, Department of Radiology, Shiraz University of Medical Sciences, Shiraz, Iran

ARTICLE INFO

Article history:
Received 24 November 2021
Accepted 13 July 2022

Key words:
adipose-derived mesenchymal stem cells
cartilage regeneration
laryngeal repair
MRI tracking

ABSTRACT

Background: Stenosis and scar formation after repair of laryngeal tissue defects are serious problems that can significantly influence a patient's quality of life.
Objective: In this study, we evaluated the use of magnetic resonance imaging to assess the efficacy of adipose tissue-derived mesenchymal stem cells (ASCs) on cartilaginous regeneration in an experimental rabbit model.
Methods: Ten male white Dutch rabbits each had a 5 mm cartilaginous defect created surgically in the right and left thyroid lamina. On the right side, ASCs labeled with iron oxide particles were infused. As a control, the left side was left untreated. Repair of the defects were then evaluated by direct observation, histological evaluation, and magnetic resonance imaging monitoring done on days 1, 7, 14, and 28.
Results: Histological examination revealed that compared with control, transplanted ASCs significantly increased cartilage regeneration ($P < 0.001$), reduced inflammation ($P < 0.001$), and fibrosis ($P = 0.050$). Magnetic resonance imaging tracking showed accurate placement and viability of the infused ASCs, as evidenced by low signal intensity onT2 weighted images at the level of the right thyroid cartilage.
Conclusions: Infusion of ASCs improved laryngeal regeneration of surgically induced cartilaginous defects while decreasing fibrous tissue formation in this in vivo rabbit model. Furthermore, magnetic resonance imaging was shown to be a useful, noninvasive method to track correct ASCs placement and viability in cartilage regeneration in this animal model.

Introduction

Stenosis and scar formation during the healing of cartilaginous laryngeal defects are major clinical problems that can seriously influence a patients' quality of life, and even survival. With varying degrees of success, numerous medications, materials, and techniques have been used to minimize or prevent scarring and restenosis following laryngeal repair.[1]

Mesenchymal stem cells (MSCs) are widely used in regenerative medicine and have shown promise in the treatment of cartilaginous defects.[2,3] MSCs can be isolated from various tissues, including bone marrow,[4,5] adipose tissue,[6,7] dental pulp,[8] synovium,[9] placenta,[10] and umbilical cord blood.[11] MSCs can be made to proliferate and differentiate into cells of mesodermal origin, such as adipocytes, osteocytes, and chondrocytes.[12,13] MSCs have local immunomodulatory properties on the innate and adaptive immune systems.[14–16] As a result of their lack of certain cell surface markers (eg, CD-14, CD-34, CD-45, and HLA-DR), MSCs have low immunogenicity.[12,14,16,17]

Immunomodulatory features of MSCs improve the tissue microenvironment for cellular proliferation and differentiation.

* Address correspondence to: Kamyar Iravani, MD, Otolaryngology Research Center, Department of Otolaryngology, Shiraz University of Medical Sciences, Khalili Hospital, Khalili St, Shiraz, Iran, Postal code: 71936-16641.
E-mail address: iravanika@sums.ac.ir (K. Iravani).

https://doi.org/10.1016/j.curtheres.2022.100682

MSCs may influence host microenvironment conditions via Toll-like receptors (TLRs). MSCs express some TLRs, including TLR2, TLR3, TLR4, TLR7, and TLR9.[14,18,19] Inflammatory molecules and pathogens can also stimulate TLRs resulting in release of TLR ligands and activation of MSCs. The type of receptors stimulated determines the response of activated MSCs. For instance, TLR3 stimulation activates an anti-inflammatory response and TLR4 stimulation activates a proinflammatory reaction of MSCs.[14,20,21]

We evaluated the efficacy of adipose tissue-derived mesenchymal stem cells (ASCs) in the healing of cartilaginous laryngeal defects in an animal model because of the limitations of doing histopathological examinations in human beings and the lack of approval for the use of ASCs for this indication in human beings. In addition to histopathology, serial magnetic resonance imaging (MRI) scans were used to noninvasively examine the viability and retention of infused ASCs.

Materials and Methods

This study utilized some previously described non-MRI methods to evaluate animal cartilage regeneration.[22]

Animal preparation

Ten male white Dutch rabbits aged 5 to 6 months with mean (SD) weight 2.20 (0.2) kg, were obtained from the Center of Comparative and Experimental Medicine (Shiraz, Iran). Individual rabbits were kept at the animal laboratory center of Shiraz University of Medical Sciences under controlled conditions, including temperature (20°C ±2°C), humidity, a 12-hour light/dark cycle every day, and free access to food and water. The study protocols were approved by the local Ethics Committee of Shiraz University of Medical Sciences (IR.SUMS.MED.REC.1398.178) and performed according to regulations of the Animal Care Committee of Veterinary Medicine, Shiraz University.

In the operating room, after induction of anesthesia by intramuscular injection of ketamine (44 mg/kg) (Alfasan, Woerden, the Netherlands) and xylazine (10 mg/kg) (Rompun; Bayer AG, Leverkusen, Germany), a small horizontal incision was made over the thyroid cartilage, and the strap muscles were separated from the midline to expose the thyroid cartilage. On both the right and left thyroid lamina, 5-mm diameter circular symmetric cartilage defects were produced using a punch device (IndiaMART, Tamil Nadu) with a round, cupped head to accurately excise and remove cartilage. On both sides, the inner perichondrium remained intact.

Cell isolation

We used allogeneic stem cells in our study. For isolation of MSCs, a single 2.2-kg male white Dutch rabbit was selected in addition to the 10 rabbits mentioned above. Under general anesthesia with ketamine and xylazine, the area between the shoulders on the back was shaved and disinfected with povidone-iodine solution (10%). A 5-cm incision was made on the skin, and 4 g subcutaneous adipose tissue was removed. The incision site was sutured together and postsurgical antibiotics (streptomycin, 3×10^6 U/d) given for 3 days.

The adipose tissue collected was then washed 3 times with phosphate-buffered saline (PBS) containing 1% penicillin G-streptomycin (10,000 U/mL).

Cell culture

The adipose tissue sample was chopped into pieces (2×2 mm) and digested in 0.2% collagenase type II (Sigma-Aldrich, St Louis, Missouri) at 37°C for 40 minutes on a shaker. The mixture was then filtered and centrifuged for 5 minutes, at 1200 rpm at room temperature. The pellet was transferred into a 5-mL tube containing Dulbecco's Modified Eagle Medium F-12 (DMEM/F-12) (Gibco, Waltham, Massachusetts) supplemented with 10% fetal bovine serum and 1% penicillin-streptomycin.

The suspension was placed in an incubator with 5% carbon dioxide and saturated humidity for 72 hours. Then, the culture media was washed with PBS and resuspended in a 4 mL new DMEM media supplemented with 10% fetal bovine serum, 1% penicillin-streptomycin (1 mL in 99 mL culture media), and 2 mM L-glutamine (Sigma-Aldrich, St Louis, Missouri). The medium was changed every 3 days until the cell density reached 80% to 90% of confluence. The logarithmic growth phase cells were assessed by calculating the cell doubling time and counting using a hemocytometer.[23] All cells were suspended and then frozen in a solution containing 10% dimethyl sulfoxide (MP Biomedicals, Santa Ana, California) and 90% PBS. The cell suspension was aliquoted into sterile plastic cryo-vials, and the date, passage number, and freezing serial number were recorded. The vials were all sealed and kept at –20°C for 60 minutes, and then they were transferred to –80°C for 24 hours and ultimately into liquid nitrogen for storage.

For subculturing, cryo-vials were taken out of the liquid nitrogen tank and quickly thawed in the water bath at 37°C. When the ice clump was thawed, 1 mL cell culture medium (88% DMEM, 10% PBS, and 1% penicillin-streptomycin) was added and centrifuged at 1200 rpm and at room temperature. The cells were transferred to a culture flask while being gently blown into a uniform single cell suspension[24] and put into an incubator at 37°C, with 5% carbon dioxide and saturated humidity. At each passage, the morphology and the amount of adherence to plastic of the ASCs was using a microscope (Nikon, ECLIPSE, TS100-F, Tokyo, Japan).[25]

Cell characterization

Cells were subcultured similarly up to the fourth passage, and at the end of each passage, the live and dead cells were counted with a Neubauer chamber, and the cells were stained with trypan blue. To determine the growth behavior in vitro at the fourth passage, purified cells were seeded into 2 12-well culture plates at the initial density of 3.75×10^4 cells per well. Then, the cells of 3 wells were counted every 24 hours for 8 days, and the mean number of cells at each time point was calculated. To determine the population doubling time, the measured values were calculated using the following formula: $[T \times (\ln 2)] / [\ln (Xe / Xb)]$ where Xe, Xb, and T were the cell number at the end point, cell number at starting point, and the incubation time in any unit, respectively.

Real-time polymerase chain reaction (RT-PCR) was used to assess the expression of markers on the ASCs and confirm that the cells were mesenchymal. After total RNA was extracted using the column RNA isolation kit (DENAzist-Asia, Mashhad, Iran) according to the manufacturer's instructions, the concentration of total RNA was measured using nanodrop spectrophotometry.[26] A complementary DNA (cDNA) was provided from the RNA samples using AccuPower Cycle Script RT PreMix Kit (BioneerCo, Daejeon, Korea) as described by the manufacturer. In brief, 15 μL total RNA was used for each reaction to reach a volume of 20 μL with diethylpyrocarbonate-treated water. Twelve thermal cycles were performed as follows: 30 seconds at 20°C for annealing, 4 minutes at 42°C for cDNA synthesis, 30 seconds at 55°C for melting secondary structure and cDNA synthesis, and 5 minutes at 95°C for inactivation.

In the next step, 1 μL template (ie, cDNA) was mixed with PCR buffer, deoxynucleoside triphosphate, magnesium dichloride, water, Taq DNA polymerase, and both forward and reverse primers. The primer sequences are as follows:

CD73 (sense 5≠ TACACCGGCAATCCACCTTC- 3´

Antisense 5≠ CTTGGGTCTTCGGGAATGCT- 3´) approximately 212 bp, CD34 (sense 5≠ ACCATCTCAGAGACTAGAGTC- 3´

Antisense 5≠ GAAAGTTCTGTTCTGTTGGC- 3´) approximately 512 bp, CD45 (sense 5≠ CAGTACTCTGCCTCCCGTTG- 3´

Antisense 5≠ TACTGCTGAGTGTCTGCGTG) approximately 269 bp

The microtubules containing 20 μL mixture were transferred to a thermocycler (Mastercycler Gradient; Eppendorf, Hamburg, Germany). Thirty amplification cycles were done, including 30 seconds of denaturation at 95°C, 30 seconds of annealing at 64°C, and 30 seconds of extension at 72°C with 2 minutes at 95°C for primary denaturation and 5 minutes at 72°C for the final extension. PCR products were evaluated for the presence of any bands using gel electrophoresis and DNA-safe stain in a 1.5% agarose gel medium. Ultraviolet radiation was used[27] to visualize the bands obtained and then the bands were evaluated using a gel documentation system (UVitec, Cambridge, United Kingdom).[28]

For chondrogenic induction and cell characterization, about 1×10^4 ASCs were transferred to a 35-mm culture dish (Corning, Berlin, Germany) containing control media composed of DMEM supplemented with 10% fetal bovine serum, 1% penicillin-streptomycin, and 1% L-glutamine and the chondrogenic media of DMEM, 10% fetal bovine serum, 1% penicillin-streptomycin, 50 μg/mL ascorbic acid, 5 ng/mL fibroblast growth factor-2, 100 ng/mL insulin growth factor, and 6.25 μg/mL transferrin. The medium was replaced every 3 days. After 3 weeks, the cultures were fixed with 10% buffered formalin for 15 minutes, and the cells were stained using conventional hematoxylin-eosin and Alcian blue methods. The cell layers were then observed using a light microscope.[29]

Cell labeling

Labeling was done using dextran-coated superparamagnetic iron oxide nanoparticles (SPIONs) (3.5 mg/mL) for 48 hours.[30] SPIONs are approved materials for cell labeling and tracking by MRI.SPIONs provide sufficient labeling without any cellular damage or functional interference.[31,32] After incubation, 3 PBS washes were performed to eliminate excess nanoparticles. To determine the absorption efficiency of iron oxide particles in vitro, cells were treated for 30 minutes with Perl's reagent (Shimi Pajoohesh, Tehran, Iran) and then counterstained with nuclear fast red. Using 95% ethanol and 10% formalin, cells labeled with iron oxide particles were fixed and permeabilized for 20 minutes at room temperature. Then, the cells were subjected to a solution made of a 1 to 1 ratio of 20% aqueous solution of hydrogen chloride and 10% aqueous solution of potassium ferrocyanide at room temperature for 20 minutes.[33]

MRI protocol

MRI was used to evaluate how well the transfused, labeled stem cells incorporated into the rabbits' laryngeal defects was a clinical 1.5 T MRI scanner (1.5 Tesla Magnetom MRI units, Siemens, Erlangen, Germany). Images were acquired with the following parameters: slice thickness: 3 mm, repetition time: 460 milliseconds, echo time: 24 milliseconds, magnetic field strength: 1.5, flip angle: 25, matrix size: 256×224, the field of view: 220×220. In each case, images were acquired in orthogonal planes. T1 and T2 weighted images were used to show the anatomy. Due to iron's susceptibility impact, the T2* sequence was applied to emphasize the injection location and confirm the presence of iron inside the tissue. Each picture was examined for low signal intensity induced by the excessive T2 shortening influence of SPION-labeled cells in the recipient tissue.[34]

Animal procedures

After the induction of the laryngeal defects as described above, labeled ASCs (2.5×10^7) were infused into the right thyroid cartilage lamina defect. Left side laryngeal defects were used as controls, and no infusion was performed on the left. Then, the treatment and control sides were covered with approximated strap muscles using 4–0 chromic sutures. The skin incision was sutured with nylon 5–0. Prophylactic antibiotic treatment (streptomycin, 3×10^6 units/d) was given to all animals for 3 days.

MRI images were taken on days 1, 7, 14, and 28. To perform histologic evaluations, 3, 3, and 4 animals were sacrificed on postoperative days 7, 14, and 28, respectively. Laryngeal specimens were harvested after euthanasia by carbon dioxide inhalation by surgical excision,[35] and preserved in 10% formalin. Specimens were sectioned (5 μm thickness) and stained with hematoxylin-eosin and Masson trichrome after a visual inspection. The presence of iron particles was confirmed by staining with iron pearls.[36]

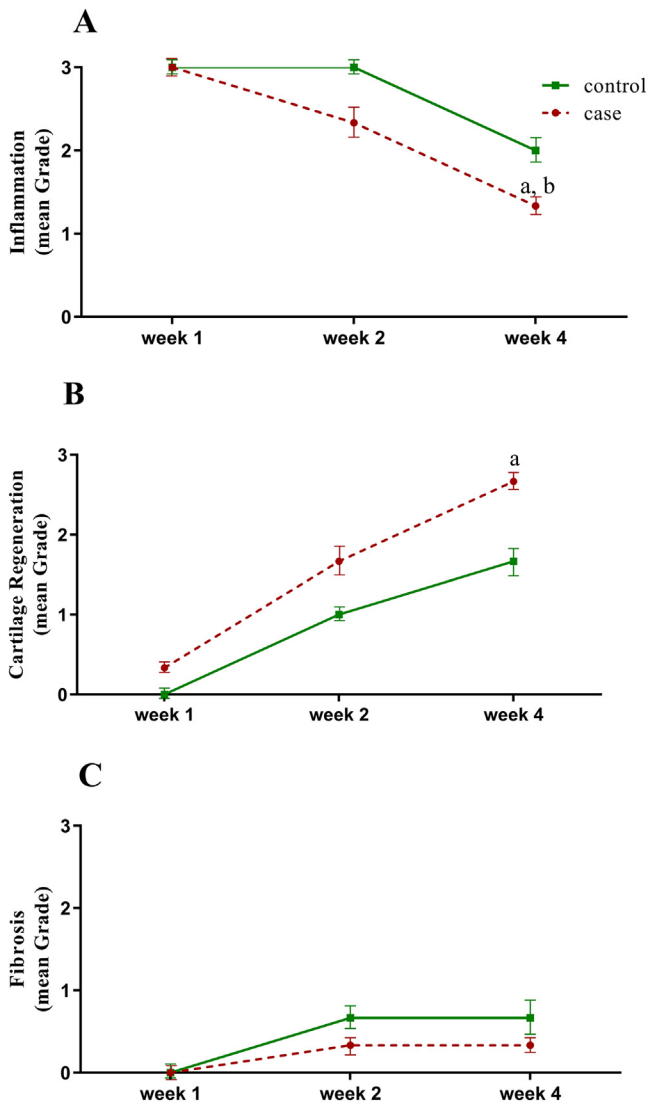

Figure 1. (A) Inflammation, (B) cartilage regeneration, and (C) fibrosis mean (SD) during 7, 14, and 28 days following adipose-derived mesenchymal stem cells application (repeated measures ANOVA and Tukey multiple comparisons test) $^aP < 0.001$ represents a significant difference between week 4 versus week 1 in the case group. $^bP < 0.05$ represents a significant difference between week 4 versus week 2 in the case group.

Table 1
Histopathological criteria for inflammation, cartilage regeneration, and fibrosis grading

Grade	Inflammatory cells	Cartilage regeneration (%)	Fibrosis (μ)
0	0–10	<25	0
1	11–50	25–50	<400
2	51–100	51–75	400–800
3	>100	>75	>800

Histologic criteria

For histopathological evaluation, we used criteria of inflammation, cartilage regeneration, and fibrosis for cartilage healing following ASCs placement. Inflammation was evaluated by the number of inflammatory cells (mainly chronic cell types such as lymphocytes, plasma cells, and histiocytes) per microscopic field (× 10). Cartilage regeneration was estimated by the percentage of defect area covered by newly formed hyaline cartilage. Fibrosis was assessed by the thickness of fibrous tissue on the micrometer scale in the defect area.[22,37] Histologic examination was done by an expert pathologist masked as to the treatment side. Histologic criteria grading is shown in Table 1.

Statistical analysis

We used repeated measures ANOVA and Tukey multiple comparisons test for statistical analyses. P values < 0.05 were considered to be statistically significant.

Table 2
Case (ie, treated) and control numbers of different types of inflammation, cartilage regeneration, and fibrosis grades for each group and week.

Variable	Week	Group	Grade			
			0	1	2	3
Inflammation	1	Case	0	0	0	3
		Control	0	0	0	3
	2	Case	0	0	2	1
		Control	0	0	0	3
	4	Case	0	2	1	0
		Control	0	0	3	0
Cartilage regeneration	1	Case	2	1	0	0
		Control	3	0	0	0
	2	Case	0	1	2	0
		Control	1	1	1	0
	4	Case	0	0	1	2
		Control	0	1	2	0
Fibrosis	1	Case	3	0	0	0
		Control	3	0	0	0
	2	Case	2	1	0	0
		Control	1	2	0	0
	4	Case	2	1	0	0
		Control	1	2	0	0

Results

Histological findings

The regenerative effects of ASCs on cartilage healing are summarized in Table 2; showing the distribution of results for treated and control groups on days 7, 14, and 28. Results are shown for inflammation, cartilage regeneration, and fibrosis indexes. ASCs infu-

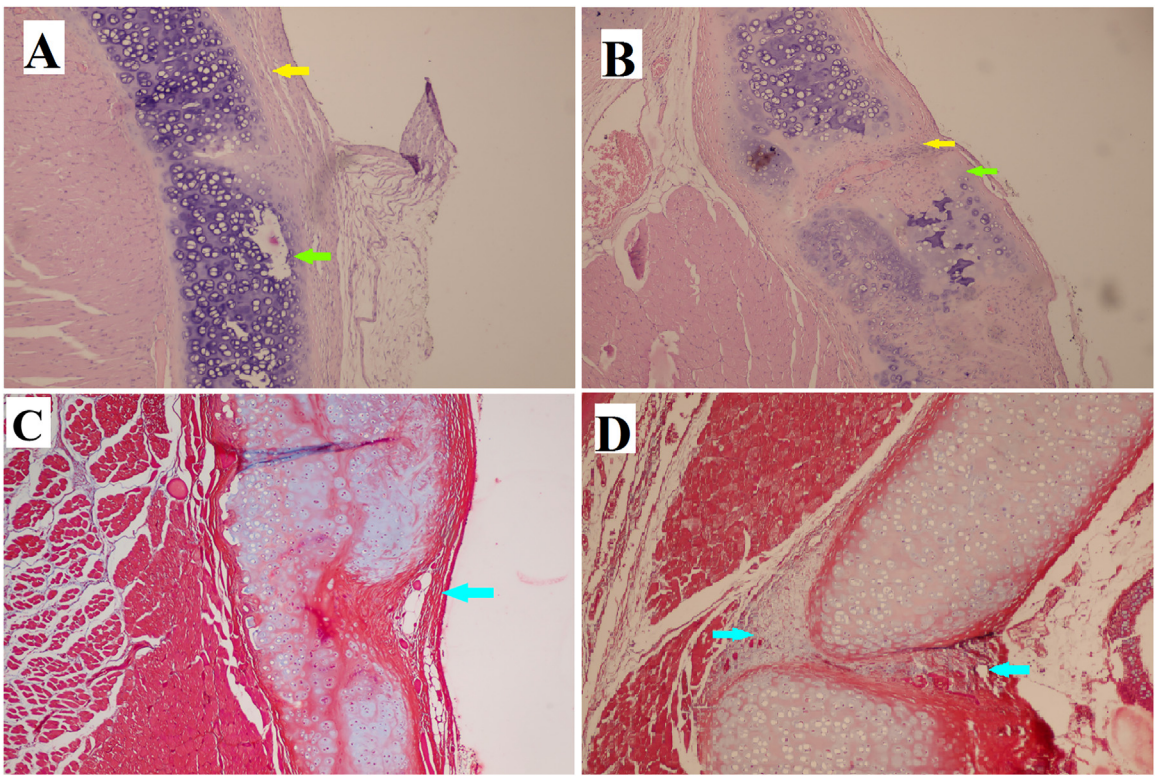

Figure 2. (A) Focal regeneration of cartilage (green arrow). (B) There was more tissue inflammation with destruction of cartilaginous tissue in control group. (A and B) Hematoxylin-eosin stain (× 100). (C and D) There was no difference regarding collagen deposition as seen using Masson trichrome stain (× 100). Inflammation is indicated by the yellow arrows, cartilage regeneration is indicated by the green arrows, and fibrosis or collagen deposition is indicated by the blue arrows.

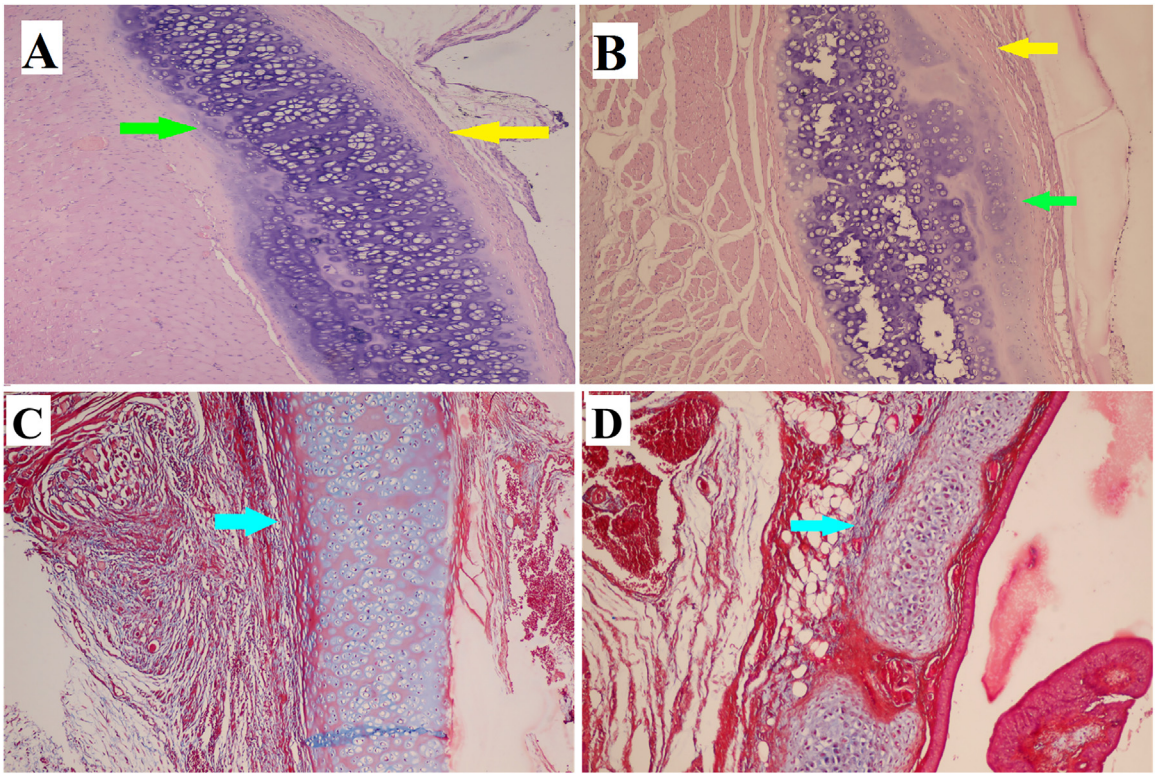

Figure 3. (A) The healing of cartilaginous defect is obvious in the case group. (B) In the control group, inflammation with cartilage defect is seen. (A and B) Hematoxylin-eosin stain (× 100). (C and D) The collagen deposition is indicated by the blue arrow as shown by Masson trichrome stain (× 100). Inflammation is indicated by the yellow arrow, cartilage regeneration is indicated by the green arrows, and fibrosis or collagen deposition are indicated by the blue arrows.

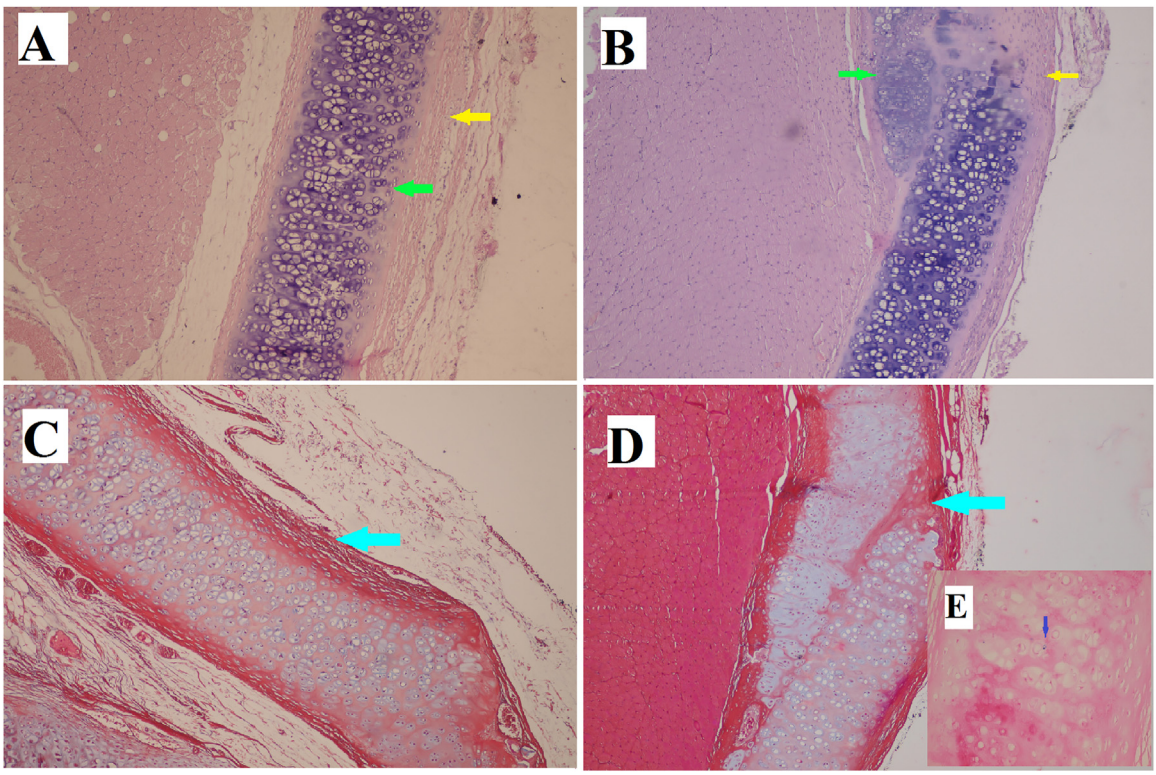

Figure 4. (A) The defect is completely replaced by normal tissue in the stem cell treated group. (B) In the control group, the defect is not completely replaced with normal tissue. (A and B) Hematoxylin-eosin stain (× 100). (C and D) The collagen deposition is more obvious in the control group, as shown by Masson trichrome stain (× 100). Inflammation is indicated by the yellow arrows, cartilage regeneration is shown by the green arrows, fibrosis or collagen deposition are shown by the blue arrows. (E) Iron particles (blue dot) are present in the chondrocyte lacuna.

sion was shown to significantly decrease inflammation ($P < 0.001$) (Figure 1A) and fibrosis ($P = 0.050$) (Figure 1C), and to improve cartilage regeneration ($P < 0.001$) (Figure 1B).

At the end of the first week after the administration of ASCs, infiltration of inflammatory cells, mostly chronic inflammatory cells, was noted on both the treated side (Figure 2A and 2C) and the opposite side (control side) (Figure 2B and 2D) of the cartilage defect. However, the extent of this infiltration was greater on the control side. By the end of the second week, cartilage repair was more apparent on the ASCs treated side (Figure 3A and 3C), and inflammation was decreased more than on the control side (Figure 3B and 3D). At the end of the fourth week, more cartilaginous repair with less fibrosis and inflammation was observed on the ASCS treated side (Figure 4A and 4C) than on the control side (Figure 4B and 4D). The presence of iron particles in the chondrocyte lacunae was confirmed by iron staining (Figure 4E).

MRI findings

Gradient echo T2 images in axial and coronal planes that were obtained at 7-day intervals for 1 month were reviewed by a radiologist who was blind to which side was the treated side and which was the control side. Axial T2 and T2* images demonstrated normal anatomy before infusion (Figure 5A and 5B).

The presence of iron was clearly confirmed on postinjection images, evident as low signal intensity on T2w and T2*w images, at the level of the thyroid cartilage, in the right paratracheal location (Figure 5C and 5D).

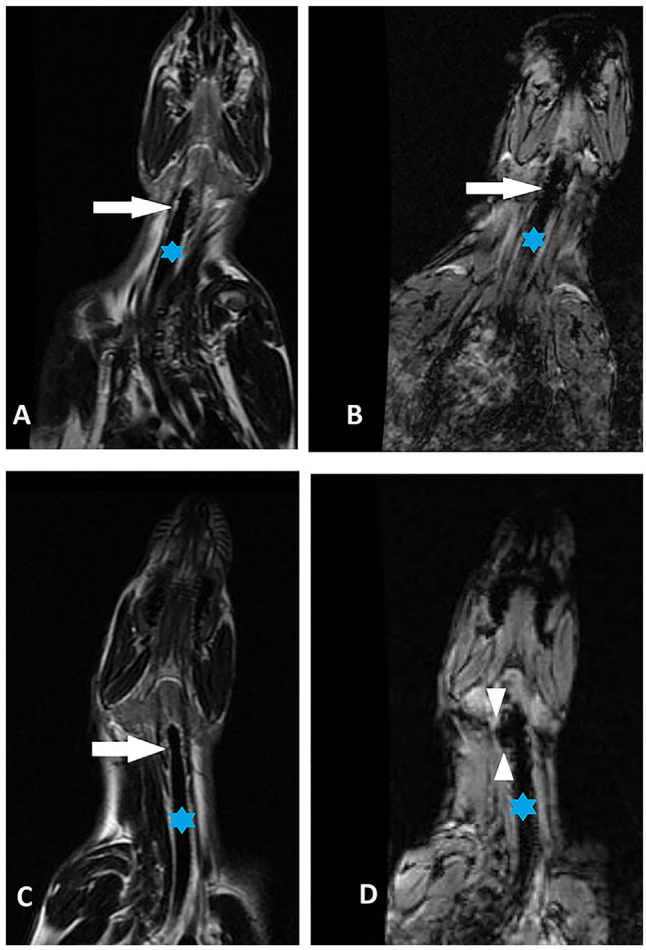

Figure 5. (A and B) Coronal T2 and T2* images of neck before injection. (A) Asterisk and white arrow indicate the trachea and level of the thyroid cartilage before injection of the nanoparticles. (B) There is no significant susceptibility artifact in paratracheal location as indicated by the arrow. (C and D) Coronal T2 and T2* images acquired 4 weeks after the injection. Asterisk and white arrow indicate the trachea and level of the thyroid cartilage after the injection of the nanoparticles. (D) T2* image confirms the presence of iron nanoparticles (small arrowheads) at the injection site in the right paratracheal location.

Discussion

This study suggests that ASCs significantly promoted laryngeal repair of surgically created cartilaginous defects in this rabbit model. This repair was accompanied by minimal scar tissue formation. The results also demonstrated the valuable role of MRI in tracking the repair, demonstrating that the ASCs were correctly placed. MRI was also useful to track the fate of infused ASCs.

MRI is a noninvasive tool that can help monitoring placement and integration of transplanted stem cells in the target area.[38–40] SPIONs were used as a contrast agent for MRIs in clinical and experimental situations. These nanoparticles, especially when coated by dextran polysaccharide, have little or no effect on cell division, viability, survival, and function of labeled cells.[41–43] SPIONs have also been approved by the Food and Drug Administration as safe contrast agents for MRI.[44]

Some studies have reported that labeled stem cells can interfere with chondrogenic and osteogenic differentiation,[45] but other studies have not shown any inhibitory effect of SPIONs on stem cell differentiation to chondroblasts and osteoblasts.[46,47] The histopathology results presented here suggest that there was an absence of interference of SPIONs stem cell labeling on cartilage differentiation. The results suggest ASCs have the potential to increase cartilage regeneration. In addition to having the ability to transform bone, cartilage, muscle, and adipose tissue in ASCs, like other MSCs, can be harvested in large quantities with minimal donor morbidity.[12]

Numerous studies have been performed on the use of ASCs in the treatment of degenerative cartilage and bone diseases, such as hip and knee osteoarthritis,[48,49] as well as cardiac diseases such as ischemic heart disease.[50]

Among the characteristics that make ASCs suitable for transplantation, especially the allogenic type, is low immunogenicity in terms of the low expression of major histocompatibility complex class II molecules.[51,52]

Among the prominent features of ASCs that enhances their ability to repair tissue is their secretion of mediators that control immunomodulation, inflammation, apoptosis, and angiogenesis.[53–55] These mediators include anti-inflammatory cytokines such as interleukin (IL) 10, IL-13, prostaglandin E2 immunosuppressor, vascular endothelial growth factor messenger RNA, platelet-derived growth factor, fibroblast growth factor, leptin, and collagen-1.[56–58] Recent studies indicated the prominent and promising role of exosomes on MSCs cartilaginous regeneration.[59,60]

ASCs have a more significant immunomodulatory potential than bone marrow-derived MSCs. The potential immunomodulation ability of ASCs has been suggested to be related to secretion of cytokines such as IL-6 and transforming growth factor-β1.[61]

A strength of our study is the histopathological examination and confirmation of the effect of ASCs on cartilaginous regeneration. Moreover, the practical application of MRI tracking for transplanted cells has benefits compared with histological confirmation alone. Among the potential drawbacks of this study was the short (1 month) duration of the investigation. However, the histologic alterations demonstrated on cartilage healing, suggests this is not a major issue. Being a preclinical animal (ie, rabbit) model is another limitation. However, these limitations must be viewed in light of the nature of the research, ethical issues, and the statistical significance of the findings.

Conclusions

Laryngotracheal stenosis and scarring are major clinical concerns. These results suggest that ASC perfusion of cartilaginous laryngeal defects may have the potential to promote cartilage regeneration while decreasing fibrous tissue formation. This study also showed the potential of MRI tracking to confirm correct ASC placement and viability. This experimental pilot study can be used to support future preclinical and then clinical trials.

Declaration of Competing Interest

The authors have indicated that they have no conflicts of interest regarding the content of this article.

Acknowledgments

This work was financially supported by Shiraz University of Medical Sciences (grant No. 16620). The authors thank native editors of the Native English Edit Company (London, United Kingdom) and Radan English Edit Manager, the exclusive representative of this company in Iran, for valuable comments in editing the manuscript.

K. Iravani and D. Mehrabani contributed to the design, drafted the manuscript, did the final approval, and accepted the accountability for the overall work. A. Doostkam and N. Azarpira contributed to the data analysis, revised the manuscript, did the final approval, and accepted accountability for the general result. P. Iranpour, M. Bahador, and S. Mehravar contributed to data collection, revised the manuscript, did the final approval, and accepted accountability for the overall work.

References

1. Lorenz RR. Adult laryngotracheal stenosis: etiology and surgical management. *Current opinion in otolaryngology & head and neck surgery*. 2003;11(6):467–472. doi:10.1097/00020840-200312000-00011.
2. Castro-Viñuelas R, Sanjurjo-Rodríguez C, Piñeiro-Ramil M, Hermida-Gómez T, Fuentes-Boquete IM, de Toro-Santos FJ, Blanco-García FJ, Díaz-Prado SM. Induced pluripotent stem cells for cartilage repair: current status and future perspectives. *European cells & materials*. 2018;36:96–109. doi:10.22203/eCM.v036a08.
3. Ma Q, Liao J, Cai X. Different Sources of Stem Cells and their Application in Cartilage Tissue Engineering. *Current stem cell research & therapy*. 2018;13(7):568–575. doi:10.2174/1574888x13666180122151909.
4. Iravani K, Sobhanmanesh A, Ashraf MJ, Hashemi SB, Mehrabani D, Zare S. The Healing Effect of Conditioned Media and Bone Marrow-Derived Stem Cells in Laryngotracheal Stenosis: A Comparison in Experimental Dog Model. *World journal of plastic surgery*. 2017;6(2):190–197.
5. Wakitani S, Imoto K, Yamamoto T, Saito M, Murata N, Yoneda M. Human autologous culture expanded bone marrow mesenchymal cell transplantation for repair of cartilage defects in osteoarthritic knees. *Osteoarthritis and cartilage*. 2002;10(3):199–206. doi:10.1053/joca.2001.0504.
6. Minteer D, Marra KG, Rubin JP. Adipose-derived mesenchymal stem cells: biology and potential applications. *Advances in biochemical engineering/biotechnology*. 2013;129:59–71. doi:10.1007/10_2012_146.
7. Bacakova L, Zarubova J, Travnickova M, Musilkova J, Pajorova J, Slepicka P, Kasalkova NS, Svorcik V, Kolska Z, Motarjemi H, Molitor M. Stem cells: their source, potency and use in regenerative therapies with focus on adipose-derived stem cells - a review. *Biotechnology advances*. 2018;36(4):1111–1126. doi:10.1016/j.biotechadv.2018.03.011.
8. Stanko P, Altanerova U, Jakubechova J, Repiska V, Altaner C. Dental Mesenchymal Stem/Stromal Cells and Their Exosomes. *Stem cells international*. 2018;2018:8973613. doi:10.1155/2018/8973613.
9. Kubosch EJ, Lang G, Furst D, Kubosch D, Izadpanah K, Rolauffs B, Sudkamp NP, Schmal H. The Potential for Synovium-derived Stem Cells in Cartilage Repair. *Current stem cell research & therapy*. 2018;13(3):174–184. doi:10.2174/1574888x12666171002111026.
10. Lin SC, Liou YM, Ling TY, Chuang YH, Chiang BL. Placenta-Derived Mesenchymal Stem Cells Reduce the Interleukin-5 Level Experimentally in Children with Asthma. *International journal of medical sciences*. 2019;16(11):1430–1438. doi:10.7150/ijms.33590.
11. Jaing TH. Umbilical cord blood: a trustworthy source of multipotent stem cells for regenerative medicine. *Cell transplantation*. 2014;23(4-5):493–496. doi:10.3727/096368914x678300.
12. Ntege EH, Sunami H, Shimizu Y. Advances in regenerative therapy: A review of the literature and future directions. *Regenerative therapy*. 2020;14:136–153. doi:10.1016/j.reth.2020.01.004.
13. Squillaro T, Peluso G, Galderisi U. Clinical Trials With Mesenchymal Stem Cells: An Update. *Cell transplantation*. 2016;25(5):829–848. doi:10.3727/096368915x689622.
14. Jiang W, Xu J. Immune modulation by mesenchymal stem cells. *Cell proliferation*. 2020;53(1):e12712. doi:10.1111/cpr.12712.
15. Kim N, Cho SG. Clinical applications of mesenchymal stem cells. *The Korean journal of internal medicine*. 2013;28(4):387–402. doi:10.3904/kjim.2013.28.4.387.
16. Ullah I, Subbarao RB, Rho GJ. Human mesenchymal stem cells - current trends and future prospective. *Bioscience reports*. 2015;35(2). doi:10.1042/bsr20150025.
17. Naji A, Eitoku M, Favier B, Deschaseaux F, Rouas-Freiss N, Suganuma N. Biological functions of mesenchymal stem cells and clinical implications. *Cellular and molecular life sciences. CMLS*. 2019;76(17):3323–3348. doi:10.1007/s00018-019-03125-1.
18. Zhao X, Liu D, Gong W, Zhao G, Liu L, Yang L, Hou Y. The toll-like receptor 3 ligand, poly(I:C), improves immunosuppressive function and therapeutic effect of mesenchymal stem cells on sepsis via inhibiting MiR-143. *Stem cells (Dayton, Ohio)*. 2014;32(2):521–533. doi:10.1002/stem.1543.
19. Tomchuck SL, Zwezdaryk KJ, Coffelt SB, Waterman RS, Danka ES, Scandurro AB. Toll-like receptors on human mesenchymal stem cells drive their migration and immunomodulating responses. *Stem cells (Dayton, Ohio)*. 2008;26(1):99–107. doi:10.1634/stemcells.2007-0563.
20. Wang Y, Chen X, Cao W, Shi Y. Plasticity of mesenchymal stem cells in immunomodulation: pathological and therapeutic implications. *Nature immunology*. 2014;15(11):1009–1016. doi:10.1038/ni.3002.
21. Kolaczkowska E, Kubes P. Neutrophil recruitment and function in health and inflammation. *Nature reviews Immunology*. 2013;13(3):159–175. doi:10.1038/nri3399.
22. Iravani K, Mehravar S, Bahador M, Azarpira N. The Healing Effect of Amniotic Membrane in Laryngeal Defects in Rabbit Model. *The Laryngoscope*. 2021;131(2):E527–e533. doi:10.1002/lary.28745.
23. Voga M, Kovač V, Majdic G. Comparison of Canine and Feline Adipose-Derived Mesenchymal Stem Cells/Medicinal Signaling Cells With Regard to Cell Surface Marker Expression, Viability, Proliferation, and Differentiation Potential. *Front Vet Sci*. 2021;13(7):610240. doi:10.3389/fvets.2020.610240.
24. Zhang J, Yun S, Bi J, Dai S, Du Y, Zannettino ACW, Zhang H. Enhanced multi-lineage differentiation of human mesenchymal stem/stromal cells within poly(N-isopropylacrylamide-acrylic acid) microgel-formed three-dimensional constructs. *J Mater Chem B*. 2018;28(12):1799–1814 6. doi:10.1039/c8tb00376a.
25. Xia CS, Zuo AJ, Wang CY, Wang YZ. Isolation of rabbit bone marrow mesenchymal stem cells using density gradient centrifugation and adherence screening methods. *Minerva Med*. 2013;104(5):519–525.
26. Deben C, Zwaenepoel K, Boeckx C, Wouters A, Pauwels P, Peeters M, Lardon F, Baay M, Deschoolmeester V. Expression analysis on archival material revisited: isolation and quantification of RNA extracted from FFPE samples. *Diagn Mol Pathol*. 2013;22(1):59–64. doi:10.1097/PDM.0b013e318269de3b.
27. Nejman-Faleńczyk B, Bloch S, Januszkiewicz A, Węgrzyn A, Węgrzyn G. A simple and rapid procedure for the detection of genes encoding Shiga toxins and other specific DNA sequences. *Toxins (Basel)*. 2015;13(11):4745–4757 7. doi:10.3390/toxins7114745.
28. Zhang X, Yan X, Gao P, Wang L, Zhou Z, Zhao L. Optimized sequence retrieval from single bands of temperature gradient gel electrophoresis profiles of the amplified 16S rDNA fragments from an activated sludge system. *J Microbiol Methods*. 2005;60(1):1–11. doi:10.1016/j.mimet.2004.08.015.
29. Hamid AA, Idrus RB, Saim AB, Sathappan S, Chua KH. Characterization of human adipose-derived stem cells and expression of chondrogenic genes during induction of cartilage differentiation. *Clinics (Sao Paulo)*. 2012;67(2):99–106. doi:10.6061/clinics/2012(02)03.
30. arrow M, Taylor A, García Carrión J, Mandal P, Park BK, Poptani H, Murray P, Rosseinsky MJ, Adams DJ. Co-precipitation of DEAE-dextran coated SPIONs: how synthesis conditions affect particle properties, stem cell labelling and MR contrast. *Contrast Media Mol Imaging*. 2016;11(5):362–370. doi:10.1002/cmmi.1700.
31. Song X, Gu X, Sun H, Fu C, Zhang Y, Dong P. Biomimetic Modification and In Vivo Safety Assessment of Superparamagnetic Iron Oxide Nanoparticles. *J Nanosci Nanotechnol*. 2016;16(4):4100–4107. doi:10.1166/jnn.2016.11640.
32. Unterweger H, Dézsi L, Matuszak J, Janko C, Poettler M, Jordan J, Bäuerle T, Szebeni J, Fey T, Boccaccini AR, Alexiou C, Cicha I. Dextran-coated superparamagnetic iron oxide nanoparticles for magnetic resonance imaging: evaluation of size-dependent imaging properties, storage stability and safety. *Int J Nanomedicine*. 2018;28:1899–1915 13. doi:10.2147/IJN.S156528.
33. Mieloch AA, Żurawek M, Giersig M, Rozwadowska N, Rybka JD. Bioevaluation of superparamagnetic iron oxide nanoparticles (SPIONs) functionalized with dihexadecyl phosphate (DHP). *Sci Rep*. 2020;10(1):2725. doi:10.1038/s41598-020-59478-2.
34. Neuwelt A, Sidhu N, Hu CA, Mlady G, Eberhardt SC, Sillerud LO. Iron-based superparamagnetic nanoparticle contrast agents for MRI of infection and inflammation. *AJR Am J Roentgenol*. 2015;204(3):W302–W313. doi:10.2214/AJR.14.12733.
35. AVMA Guidelines for the Euthanasia of Animals: 2020 Edition. https://www.avma.org/KB/policies/documents/euthanasia
36. Naumova AV, Balu N, Yarnykh VL, Reinecke H, Murry CE, Yuan C. MRI Tracking of Graft Survival in the Infarcted Heart: Iron Oxide Particles vs. Ferritin Over-

expression Approach. *J Cardiovasc Pharmacol Ther*. 2014;19(4):358–367. doi:10.1177/1074248414525999.
37. Cincik H, Gungor A, Cakmak A, Omeroglu A, Poyrazoglu E, Yildirim S, Cekin E, Candan H. The effects of mitomycin C and 5-fluorouracil/triamcinolone on fibrosis/scar tissue formation secondary to subglottic trauma (experimental study). *Am J Otolaryngol*. 2005;26(1):45–50. doi:10.1016/j.amjoto.2003.07.002.
38. Tangchitphisut P, Srikaew N, Phongkitkarun S, Jaovisidha S, Tawonsawatruk T. Using iron sucrose-labeled adipose-derived mesenchymal stem cells in 1.5 and 3 T MRI tracking: An in vitro study. *Heliyon*. 2020;6(8):e04582. doi:10.1016/j.heliyon.2020.e04582.
39. Ali AAA, Shahror RA, Chen KY. Efficient Labeling Of Mesenchymal Stem Cells For High Sensitivity Long-Term MRI Monitoring In Live Mice Brains. *International journal of nanomedicine*. 2020;15:97–114. doi:10.2147/ijn.S211205.
40. Zare S, Mehrabani D, Jalli R, Saeedi Moghadam M, Manafi N, Mehrabani G, Jamhiri I, Ahadian S. MRI-Tracking of Dental Pulp Stem Cells In Vitro and In Vivo Using Dextran-Coated Superparamagnetic Iron Oxide Nanoparticles. *Journal of clinical medicine*. 2019;8(9). doi:10.3390/jcm8091418.
41. Ma Y, Ji Y, You M, Wang S, Dong Y, Jin G, Lin M, Wang Q, Li A, Zhang X, Xu F. Labeling and long-term tracking of bone marrow mesenchymal stem cells in vitro using NaYF4:Yb(3+),Er(3+) upconversion nanoparticles. *Acta biomaterialia*. 2016;42:199–208. doi:10.1016/j.actbio.2016.07.030.
42. Mohanty S, Jain KG, Nandy SB, Kakkar A, Kumar M, Dinda AK, Singh H, Ray A. Iron oxide labeling does not affect differentiation potential of human bone marrow mesenchymal stem cells exhibited by their differentiation into cardiac and neuronal cells. *Molecular and cellular biochemistry*. 2018;448(1-2):17–26. doi:10.1007/s11010-018-3309-9.
43. Lu CW, Hsiao JK, Liu HM, Wu CH. Characterization of an iron oxide nanoparticle labelling and MRI-based protocol for inducing human mesenchymal stem cells into neural-like cells. *Scientific reports*. 2017;7(1):3587. doi:10.1038/s41598-017-03863-x.
44. Thakor AS, Jokerst JV, Ghanouni P, Campbell JL, Mittra E, Gambhir SS. Clinically Approved Nanoparticle Imaging Agents. *Journal of nuclear medicine: official publication, Society of Nuclear Medicine*. 2016;57(12):1833–1837. doi:10.2967/jnumed.116.181362.
45. Kostura L, Kraitchman DL, Mackay AM, Pittenger MF, Bulte JW. Feridex labeling of mesenchymal stem cells inhibits chondrogenesis but not adipogenesis or osteogenesis. *NMR in biomedicine*. 2004;17(7):513–517. doi:10.1002/nbm.925.
46. Henning TD, Gawande R, Khurana A, Tavri S, Mandrussow L, Golovko D, Horvai A, Sennino B, McDonald D, Meier R, Wendland M, Derugin N, Link TM, Daldrup-Link HE. Magnetic resonance imaging of ferumoxide-labeled mesenchymal stem cells in cartilage defects: in vitro and in vivo investigations. *Molecular imaging*. 2012;11(3):197–209.
47. Jasmin de Souza GT, Louzada RA, Rosado-de-Castro PH, Mendez-Otero R, Campos de Carvalho AC. Tracking stem cells with superparamagnetic iron oxide nanoparticles: perspectives and considerations. *International journal of nanomedicine*. 2017;12:779–793. doi:10.2147/ijn.S126530.
48. Rigotti G, Marchi A, Galiè M, Baroni G, Benati D, Krampera M, Pasini A, Sbarbati A. Clinical treatment of radiotherapy tissue damage by lipoaspirate transplant: a healing process mediated by adipose-derived adult stem cells. *Plastic and reconstructive surgery*. 2007;119(5):1409–1422. doi:10.1097/01.prs.0000256047.47909.71.
49. Kim M, Kim I, Kim SH, Jung M, Han S, Lee J, Nam JS, Lee SK, Bang S. Cryopreserved human adipogenic-differentiated pre-adipocytes: a potential new source for adipose tissue regeneration. *Cytotherapy*. 2007;9(5):468–476. doi:10.1080/14653240701358452.
50. Jayaraj JS, Janapala RN, Qaseem A, Usman N, Fathima N, Kashif T, Reddy VK, Bakshi S. Efficacy and Safety of Stem Cell Therapy in Advanced Heart Failure Patients: A Systematic Review with a Meta-analysis of Recent Trials Between 2017 and 2019. *Cureus*. 2019;11(9):e5585. doi:10.7759/cureus.5585.
51. Niemeyer P, Kornacker M, Mehlhorn A, Seckinger A, Vohrer J, Schmal H, Kasten P, Eckstein V, Südkamp NP, Krause U. Comparison of immunological properties of bone marrow stromal cells and adipose tissue-derived stem cells before and after osteogenic differentiation in vitro. *Tissue engineering*. 2007;13(1):111–121. doi:10.1089/ten.2006.0114.
52. Zhang J, Huang X, Wang H, Liu X, Zhang T, Wang Y, Hu D. The challenges and promises of allogeneic mesenchymal stem cells for use as a cell-based therapy. *Stem cell research & therapy*. 2015;6:234. doi:10.1186/s13287-015-0240-9.
53. Caplan AI. Chapter 15 - Mesenchymal Stem Cells in Regenerative Medicine. In: Atala A, Lanza R, Mikos AG, Nerem R, eds. *Principles of Regenerative Medicine (Third Edition)*. Boston: Academic Press; 2019:219–227.
54. Vizoso FJ, Eiro N, Cid S, Schneider J, Perez-Fernandez R. Mesenchymal Stem Cell Secretome: Toward Cell-Free Therapeutic Strategies in Regenerative Medicine. *International journal of molecular sciences*. 2017;18(9). doi:10.3390/ijms18091852.
55. Teixeira FG, Carvalho MM, Sousa N, Salgado AJ. Mesenchymal stem cells secretome: a new paradigm for central nervous system regeneration? *Cellular and molecular life sciences: CMLS*. 2013;70(20):3871–3882. doi:10.1007/s00018-013-1290-8.
56. Park CW, Kim KS, Bae S, Son HK, Myung PK, Hong HJ, Kim H. Cytokine secretion profiling of human mesenchymal stem cells by antibody array. *International journal of stem cells*. 2009;2(1):59–68. doi:10.15283/ijsc.2009.2.1.59.
57. Blaber SP, Webster RA, Hill CJ, Breen EJ, Kuah D, Vesey G, Herbert BR. Analysis of in vitro secretion profiles from adipose-derived cell populations. *Journal of translational medicine*. 2012;10:172. doi:10.1186/1479-5876-10-172.
58. Kokai LE, Marra K, Rubin JP. Adipose stem cells: biology and clinical applications for tissue repair and regeneration. *Translational research: the journal of laboratory and clinical medicine*. 2014;163(4):399–408. doi:10.1016/j.trsl.2013.11.009.
59. Zhang S, Chu WC, Lai RC, Lim SK, Hui JH, Toh WS. Exosomes derived from human embryonic mesenchymal stem cells promote osteochondral regeneration. *Osteoarthritis and cartilage*. 2016;24(12):2135–2140. doi:10.1016/j.joca.2016.06.022.
60. Wang Y, Yu D, Liu Z, Zhou F, Dai J, Wu B, Zhou J, Heng BC, Zou XH, Ouyang H, Liu H. Exosomes from embryonic mesenchymal stem cells alleviate osteoarthritis through balancing synthesis and degradation of cartilage extracellular matrix. *Stem cell research & therapy*. 2017;8(1):189. doi:10.1186/s13287-017-0632-0.
61. Melief SM, Zwaginga JJ, Fibbe WE, Roelofs H. Adipose tissue-derived multipotent stromal cells have a higher immunomodulatory capacity than their bone marrow-derived counterparts. *Stem cells translational medicine*. 2013;2(6):455–463. doi:10.5966/sctm.2012-0184.